frontiers | Frontiers in Materials

TYPE Original Research
PUBLISHED 06 February 2024
DOI 10.3389/fmats.2024.1361159

OPEN ACCESS

EDITED BY
Zhongya Zhang,
Chongqing Jiaotong University, China

REVIEWED BY
Qiang Pei,
Dalian University, China
Hui Chen,
Wenzhou University of Technology, China

*CORRESPONDENCE
Hu Kong,
kh980407@163.com

RECEIVED 25 December 2023
ACCEPTED 19 January 2024
PUBLISHED 06 February 2024

CITATION
Wang Y, Kong H, Sun Y, Tan M and Chen L (2024), Study on the monitoring method of debonding between concrete beams and reinforced steel plates based on piezoelectric smart materials.
Front. Mater. 11:1361159.
doi: 10.3389/fmats.2024.1361159

Study on the monitoring method of debonding between concrete beams and reinforced steel plates based on piezoelectric smart materials

Yanru Wang[1], Hu Kong[2]*, Yaxi Sun[3], Mingli Tan[4] and Lihua Chen[5]

[1]School of Civil Engineering, Taizhou University, Taizhou, China, [2]Department of Civil and Transportation Engineering, Hohai University, Nanjing, China, [3]School of Digital Economy and Information Management, Chongqing Yitong University, Chongqing, China, [4]Faculty of Architectural Engineering, Huaihua Vocationnal and Technical College, Huaihua, China, [5]Chongqing Vocational Institute of Engineering, Chongqing, China

Concrete reinforcement is essential for ensuring the safety and durability of concrete structures. Bonding steel plates to reinforce concrete is widely used to renovate or strengthen concrete beam structures. Due to construction quality and the influence of factors such as environment and fatigue, debonding often occurs between the steel plate and concrete, making monitoring and early warning after concrete structure reinforcement challenging. This paper proposes a novel approach to monitor the degree of debonding between the steel plate and concrete beam using active sensing technology. The method uses lead zirconate titanate (PZT) as an actuator to generate stress waves. It prepares strip sensors with polyvinylidene fluoride as the sensing element to monitor stress waves passing through the steel plate and concrete beam. The monitoring system detects the degree of debonding between the steel plate and the concrete beam by monitoring the change in surface voltage of the sensor. Experiments show that the degree of debonding significantly correlates with the received voltage signal; the higher the debonding, the larger the received voltage signal. It is also observed that, at the same degree of debonding, the actuator and sensor attachment position have a particular impact on the received voltage signal. Through experiments and numerical simulation analysis, it is found that when the sensor is attached to the left side of the steel plate, that is, the bonded section of the steel plate, the amplitude of the voltage signal collected by the dynamic information acquisition system is the smallest, i.e., V_debonded section > V_middle > V_bonded section. Based on the above research, the active sensing technology proposed in this paper has good sensitivity to the degree of debonding between the steel plate and concrete. It is expected to become an effective monitoring and evaluation method for the degree of debonding between steel plates and concrete.

KEYWORDS

debonding monitoring, active sensing technology, bar sensor, PZT actuator, PVDF

1 Introduction

Concrete beams, as a common transverse component, are widely used in engineering structures. During their long-term use, the components are prone to serious deformation or even cracking due to adverse factors such as external loads (Zhan, et al., 2015), corrosion (Aslani and Dehestani, 2020), fatigue (Zanuy et al., 2007), etc. If the defects in the concrete beams are not detected and repaired in a timely manner, it will seriously threaten the safety of the structure (Kaklauskas, 2017; Fu and Lao, 2023; Yang, et al., 2023).

Common methods for repairing and strengthening concrete beams include increasing section reinforcement (Ye et al., 2010; Li, et al., 2014; Naser, et al., 2019), bonding fiber-reinforced composite material (Dai, et al., 2011; Hawileh, et al., 2018; Zhang, et al., 2023), and bonding steel plate reinforcement (Barnes and Mays, 2006; Arslan, et al., 2008; Qu, et al., 2017; Ma and Liu, 2023). Among them, the method of bonding steel plate reinforcement has been widely used in concrete reinforcement due to its simple and fast construction, and it does not significantly increase the cross-sectional dimensions and weight of the reinforced components. However, the debonding of the steel plate is a common problem in the bonding steel plate reinforcement. The quality of the bonding between the steel plate and the concrete directly affects the safety of the structure (Jones, et al., 1988; Oehlers and Ali, 1998; Ali, et al., 2005; Zou, et al., 2023). Once the steel plate is detached from the concrete bonding layer, it will affect the structural load and may even cause cracks to further develop, leading to structural failure. Due to the invisibility of the bonding between the steel plate and the concrete structure, it is difficult to monitor the quality of the bonding steel plate. Currently, the widely used non-destructive testing methods, such as acoustic emission technology (Zaki, et al., 2023), ultrasonic testing technology (Shah, et al., 2009; Shah and Ribakov, 2009), fiber optic sensing technology (Buda-Ożóg et al., 2022), and digital image processing technology (Galkovski et al., 2023), all involve sophisticated equipment and complex algorithms, requiring high demands on the testing environment and the operator's skill, making them difficult to apply flexibly in some engineering applications. Therefore, there is an urgent need to find a simple and effective non-destructive monitoring method for monitoring the debonding of the steel structure and the concrete beam bonding joint.

Piezoelectric materials are commonly used in active sensing technology for structural health monitoring due to their sensing and actuating functions in recent years (Liao, et al., 2008; Howser, et al., 2011; Huo, et al., 2018). The widely used piezoelectric materials include lead zirconate titanate (PZT) and polyvinylidene fluoride (PVDF). PZT has strong piezoelectric effect (Song, et al., 2002) and a wide bandwidth (Wu, et al., 2019), while PVDF is a piezoelectric polymer that overcomes the shortcomings of piezoelectric ceramics and has the advantages of structural flexibility and stable performance (Audrain, et al., 2004). Both materials have been widely used and have shown good results in the detection of bonding slip (Qin, et al., 2015; Zeng, et al., 2015; Xu, et al., 2018) between concrete and steel, monitoring of structural impact damage (Yu, et al., 2013), and monitoring of asphalt pavement crack damage (Hasni, et al., 2017).

Due to the issue of debonding between reinforced steel plates and concrete beams, and based on the superior performance of lead zirconate titanate (PZT) and polyvinylidene fluoride (PVDF) in the field of structural detection, this paper proposes a new method for real-time monitoring of debonding between steel plates and concrete beams using PVDF as the sensor for debonding monitoring and PZT as the actuator for debonding monitoring. Through active monitoring experiments on the reinforced concrete with attached steel plates, the relationship between the received electrical signal and the degree of debonding was studied. In addition, based on experimental and numerical simulation methods, the correlation between the sensor installation position and the received electrical signal under the same debonding state was analyzed, and the mechanism was explained. Through the above research, the feasibility of the proposed method for monitoring the debonding state between reinforced steel plates and concrete beams was further validated.

2 Preparation and monitoring mechanism of piezoelectric transducer

2.1 The preparation of a bar sensor

The strip sensor is prepared based on polyvinylidene fluoride (PVDF), using a PVDF sensor element with dimensions of 1 cm × 2 cm × 28 μm. The main performance parameters of PVDF are shown in Table 1. A polydimethylsiloxane (PDMS) with an outer ring length of 7cm, inner ring length of 5cm, and a thickness of 500 μm is used as the substrate material to increase the range of the strip sensor. The mechanical performance parameters of PDMS are shown in Table 2. The detailed fabrication process of the strip sensor is as follows: silver is plated on the outer edge of the PVDF with a thickness of 1μm, then copper foil conductive tape is used to attach the shielded wire to one side of the PVDF. The PVDF is then attached to the surface of the PDMS using epoxy resin. The structural fabrication process of the strip sensor is shown in Figures 1A a photo of the actual sensor is shown in Figure 1B.

2.2 Preparation of PZT actuators

The piezoelectric actuator is prepared from lead zirconate titanate (PZT), with the common types being PZT-4, PZT-5, and PZT-8. The performance parameters of the three types of lead zirconate titanate (PZT) materials are shown in Table 3. Among them, PZT-4 piezoelectric ceramics have high dielectric constants and electromechanical coupling coefficients, making them suitable for self-excited sensors that function as both receiving and transmitting ends (Othmani, et al., 2020) PZT-5 piezoelectric ceramics have a small quality factor and high dielectric losses but exhibit high sensitivity, and are therefore commonly used as receiving elements in devices such as accelerometers, piezoelectric sensors, and ultrasonic probes (Bouche, 1975; Benes, et al., 1995; Kumar, et al., 2022). PZT-8 piezoelectric ceramics are a type of high-power piezoelectric material with low dielectric losses, suitable for large amplitude excitation, mainly used in ultrasonic cleaning and ultrasonic surgery (Prabakar, 2007; Zhang, et al., 2017). Through comparison, it is found that PZT-4 is more suitable as a driver

TABLE 1 Main performance parameters of PVDF film.

$\varepsilon/\varepsilon_0$ (KHz)	C (m/s)	Z (Kg/sm^4)	K_{33} (%)	σ_s (N/m^2)	ρ(kg/m^3)	T (°C)
9.5 ± 1.0	2000	2.5–3×10^4	10–14	44–55×10^6	1.78×10^3	−40–80

TABLE 2 PDMS film mechanical properties parameters.

T (°C)	Shore hardness (HA)	Tensile strength (MPa)	Peel strength (KN/m)	Ep (GPa)	Tearing elongation (%)	Dielectric strength (KV/mm)	k_{33}	Volume resistance (Ω·cm)
−40–200	50	4	7	1.6	100	12	2.7	10^{14}

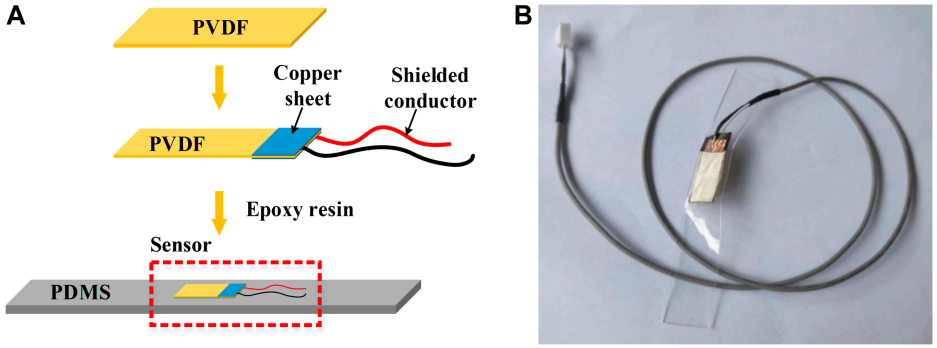

FIGURE 1
Bar Type Piezoelectric Sensor. **(A)** Preparation process diagram **(B)** Physical diagram.

TABLE 3 Mechanical properties parameters of PZT materials.

Material type	S_{11}(N·m^{-2})	d_{33} (pC/N)	$\varepsilon/\varepsilon_0$	E_p (Gpa)	k_{33}	Curie temperature T (°C)
PZT-4	1.35 × 10^{-11}	320	1,350	76.5	0.64	360
PZT-5H	2 × 10^{-11}	650	3,400	60.6	0.8	220
PZT-8	1.1 × 10^{-11}	225	1,300	60	0.63	300

for monitoring tests of bonding seam delamination in reinforced concrete beams. In this study, the selected dimensions of PZT-4 are 1 cm × 2 cm × 28 μm.

2.3 The mechanism of active monitoring for debonding between reinforced steel plate and concrete beam

Piezoelectric materials, after being polarized by an electric field, will generate charges when subjected to force, called the positive piezoelectric effect; under the influence of an electric field, deformation known as the inverse piezoelectric effect will occur. By attaching a strip sensor and PZT actuator to the steel plate, connecting PZT with the piezoelectric ceramic driving power source to generate stress waves, and connecting PVDF with the dynamic information acquisition instrument to convert the received stress waves into electrical signals. The sensing mechanism described above can be represented by the first type of piezoelectric equation as follows:

$$\boldsymbol{x} = \boldsymbol{s}^{E}\boldsymbol{X} + \boldsymbol{d}_{t}\boldsymbol{E} \tag{1}$$

$$\boldsymbol{D} = \boldsymbol{d}\boldsymbol{X} + \boldsymbol{\varepsilon}^{x}\boldsymbol{E} \tag{2}$$

Where Formula (1) represents the ability of piezoelectric materials to convert electrical energy into mechanical energy, which can be used to make PZT actuators; Formula (2) represents the ability of piezoelectric materials to convert mechanical energy into electrical energy, which can be used to make strip sensors. For

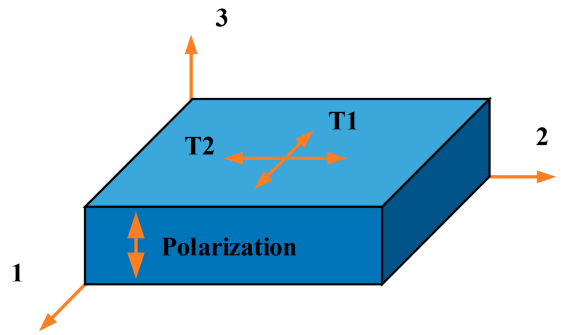

FIGURE 2
Piezoelectric material calculation orientation diagram.

the piezoelectric equations of PZT and PVDF, the piezoelectric coefficients have symmetry with respect to crystal type, so Formula (2) can be simplified to:

$$D_3 = d_{31}X_1 + d_{32}X_2 \tag{3}$$

Where 3 represents the polarization direction. When the strip sensor is subjected to the forces in the 1 and 2 directions, the charge produced in the 3 direction is D3, as shown in Figure 2.

According to the research on the piezoelectric effect of piezoelectric materials after electric field polarization by Zhao and Li (2006) when a bar sensor is subjected to mechanical force, charges will be generated on the upper and lower surfaces, with the amount of charge being:

$$Q = \iint D_3 d_x d_y \tag{4}$$

Moreover, due to the similar structure of piezoelectric materials to that of a capacitor, the voltage, after the capacitance is generated on the upper and lower surfaces, can be determined as follows:

$$U = \frac{Q}{C_q} \tag{5}$$

Where C_q represents the capacitance of piezoelectric material, which only related to the properties of the material, and the capacitance is:

$$C_q = \frac{\varepsilon bl}{t} \tag{6}$$

Where ε represents the relative dielectric constant of the ceramic sheet, and *lbt* represents the length, width, and thickness of the sensor, respectively. Therefore, by applying excitation signals to the PZT, it is possible to monitor the voltage signal output by the strip sensor, which indicates the change in surface voltage of the strip sensor in order to assess the level of debonding between the steel plate and the concrete beam.

3 Monitoring experiment and numerical simulation of debonding between reinforced steel plate and concrete beam

This section includes two sets of experiments and one set of numerical simulations to demonstrate the feasibility of the theoretical model for monitoring the debonding level between steel plates and concrete beam, as well as the effect of different sensor attachment positions on the received stress wave transmission when the debonding level of the steel plate remains the same. The first set of experiments consists of a control experiment with fixed positions of the PZT actuator and strip sensor but different debonding levels of the steel plates. The second set of experiments involves a control experiment with the same debonding level of the steel plates, but different positions of the PZT actuator and strip sensor. Additionally, numerical simulations were conducted for steel plates with different positions of the PZT actuator and sensor attachment but the same debonding level.

TABLE 4 Cracked concrete beam mix proportions.

Concrete	Sand	Aggregate	Water
416.7	624.2	1,159.1	200

3.1 The description of experiment

The apparatus used in the experiment consists of test pieces, steel plates, PZT actuators, strip sensors, DH5922N dynamic information acquisition system, HPV series piezoelectric ceramic drive power supply and signal amplifier. In order to simulate the actual use environment of the steel plate bonding reinforcement method, the test pieces include 4 cracked concrete beams, with crack dimensions of 150 mm × 150 mm × 600 mm and a mix ratio as shown in Table 4. First, when using the steel plate bonding reinforcement method for the cracked concrete beams, it is necessary to repair the cracked cracks, fill the cracks with repair adhesive using an adhesive injector to repair the concrete beams. Secondly, before reinforcing the concrete beams with steel plates, it is necessary to calculate the ultimate load-bearing capacity of the steel plate. Once the calculation meets the requirements, the steel plate is cut into the required shape, and the surface is coated with adhesive. The steel plate is then bonded to the concrete surface. After bonding the steel plate to the concrete beams, the reinforced concrete beams are cured in their natural state for 3 days to ensure a strong bond between the concrete beams and the steel plate, as shown in Figure 3.

After the concrete beams are firmly bonded to the steel plate, the strip sensor and the PZT actuator are bonded to the steel plate using epoxy resin. The strip sensor is connected to an external charge amplifier and then to the dynamic information acquisition system. The charge amplifier connected to the strip sensor is set to an amplification ratio of 100, and the voltage signal acquisition frequency of the dynamic information acquisition system is set to 500Hz. The PZT actuator is connected to the piezoelectric ceramic drive power supply, and the piezoelectric ceramic drive power supply applies a 60Hz–100Hz frequency-sweep sine signal with an amplitude of 5V to the PZT actuator as an excitation signal, with a signal duration of 10s. After the power is turned on, the signal is unstable and needs to wait for the signal to stabilize before starting the timer, then the dynamic information acquisition system is used to collect the signal.

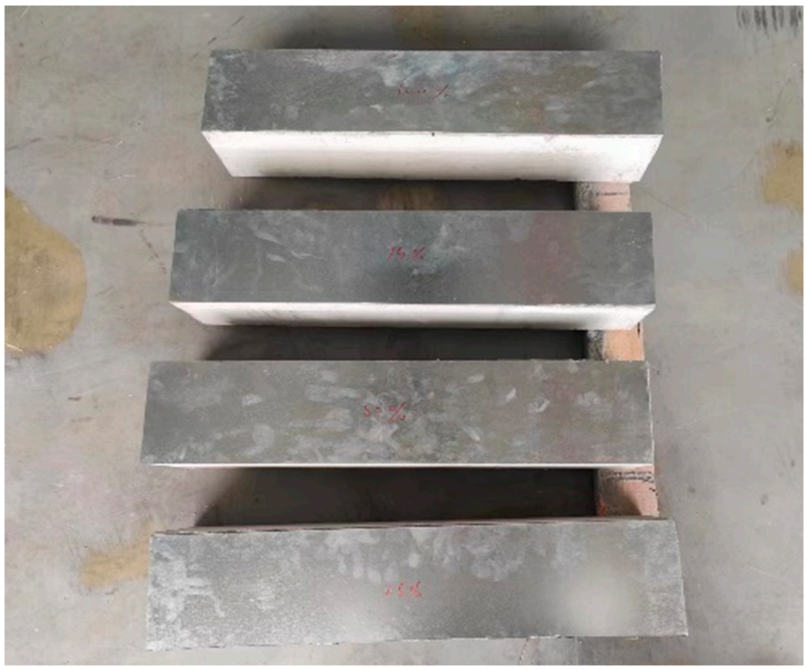

FIGURE 3
Concrete beam with cracks.

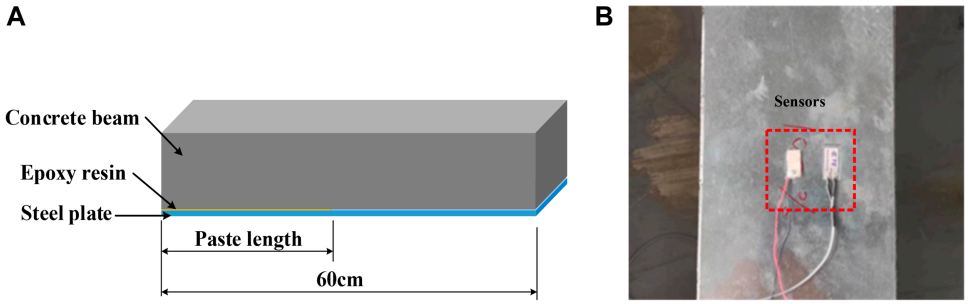

FIGURE 4
Concrete beams with different length of steel plate. **(A)** bonding steel plate reinforcement **(B)** Piezoelectric material paste.

3.2 Debonding monitoring experiment between reinforced steel plates and concrete beams

To study the signal response of piezoelectric materials to the degree of delamination of steel plates, the steel plates were bonded to four concrete beams with adhesive, with bonding lengths of 100%, 75%, 50%, and 25% of the concrete beam length, as shown in Figure 4A. Then, epoxy resin was used to bond the strip sensor and PZT actuator to the middle of the steel plate, as shown in Figure 4B. The electrical signals received by the dynamic information acquisition system are shown in Figure 5.

According to Figure 5, it can be observed that for the same frequency sweep signal, the voltage signal amplitude collected by the dynamic information acquisition instrument varies with different lengths of steel plate bonding. When the bonding length of the steel plate is 100%, the voltage signal amplitude collected by the dynamic information acquisition instrument is 0.017mV; when the bonding length is 75%, the voltage signal amplitude collected is 0.020mV; when the bonding length is 50%, the voltage signal amplitude collected is 0.080mV; and when the bonding length is 25%, the voltage signal amplitude collected is 0.103 mV.

The relationship between the length of steel plate adhesion and the voltage amplitude is shown in Figure 6. As shown in Figure 6, with the decrease in the length of steel plate adhesion, the voltage signal amplitude collected by the dynamic information acquisition instrument gradually increases, especially at a adhesive length of 75%, where a significant turning point in the signal amplitude occurs. Therefore, the characteristics of the voltage signal amplitude collected by the dynamic information acquisition instrument changing with the degree of steel plate detachment can be used to characterize the degree of detachment between the steel

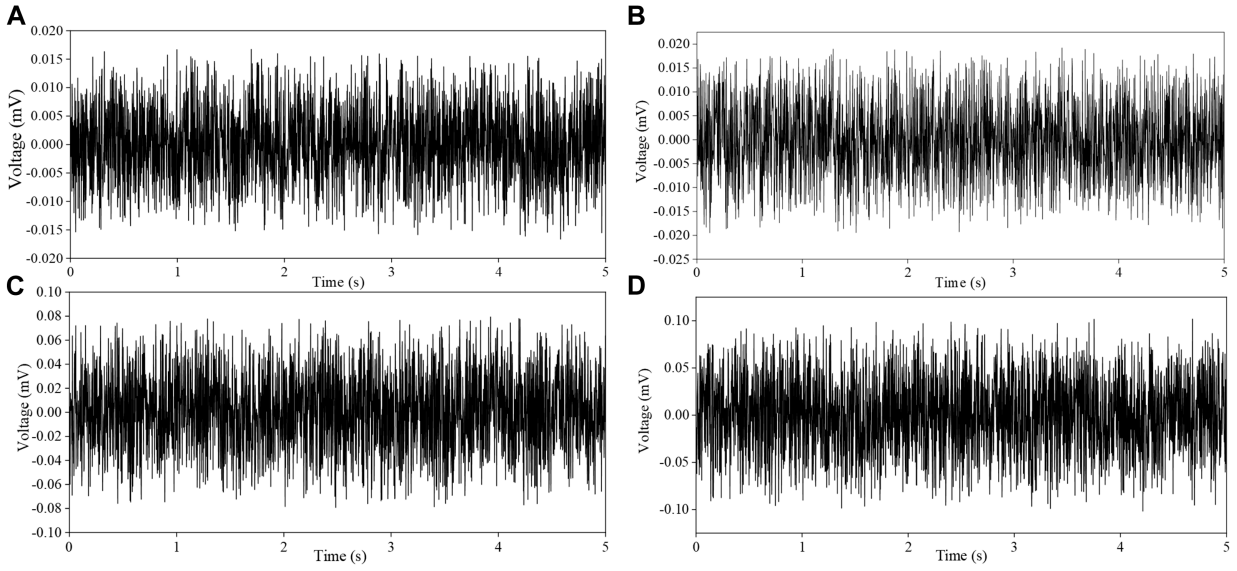

FIGURE 5
Signal response of steel plates with different sticking lengths. **(A)** Paste length 100% **(B)** Paste length 75% **(C)** Paste length 50% **(D)** Paste length 25%.

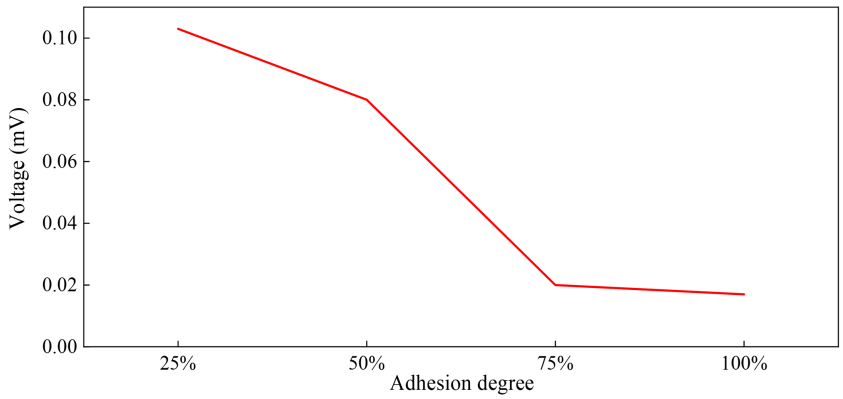

FIGURE 6
Different paste length signal amplitude change diagram.

plate and concrete; that is, the larger the signal amplitude received by the dynamic information acquisition instrument, the shorter the length of steel plate adhesion, the greater the degree of detachment between the steel plate and the concrete beam.

3.3 The experiment on the influence of different monitoring positions on the electrical signal

The monitoring experiment of the debonding degree of steel plates has proved the feasibility of the active sensing technology in monitoring the debonding degree of steel plates. However, the influence of sensor position on signal amplitude cannot be ruled out. In order to study the difference in signal amplitude caused by the different positions of sensors attached to the steel plate, a concrete beam with a steel plate attachment length of 50% was selected. PZT actuators and strip sensors were respectively attached to the left end, middle and right end of the beam, as shown in Figure 7. The dynamic information acquisition system was used to collect the signals generated by the strip sensors attached to different positions of the steel plate, as shown in Figure 8.

As seen in Figure 8, it can be observed that when the PZT actuator and strip sensor are attached to different positions on the steel plate, the voltage signal amplitudes collected by the dynamic information acquisition system are also different. When the sensor is attached to the right side of the steel plate, i.e., the debonding section of the steel plate, the voltage signal amplitude collected by

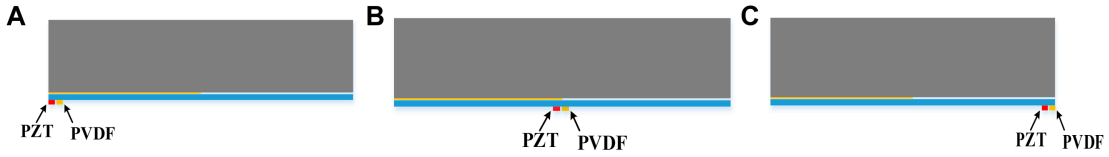

FIGURE 7
Sensors at different positions paste schematics. **(A)** left **(B)** mid **(C)** right.

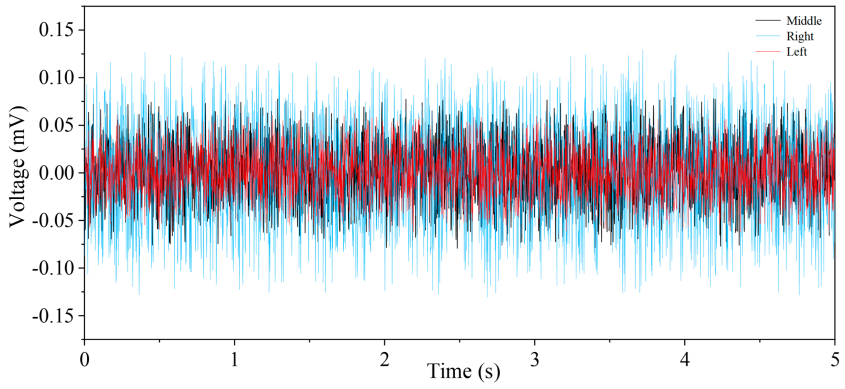

FIGURE 8
Signal response of different position sensors.

the dynamic information acquisition system is the largest. When the sensor is attached to the middle of the steel plate, the voltage signal amplitude collected by the dynamic information acquisition system is significantly smaller than that collected in the debonding section. When the sensor is attached to the left side of the steel plate, i.e., the bonding section of the steel plate, the voltage signal amplitude collected by the dynamic information acquisition system is the smallest, i.e., Vdebonding section > Vmiddle > Vbonding section. Therefore, due to the different bonding conditions between the steel plate and concrete, sensors in different positions perceive external signals differently under the same excitation signal, resulting in different signal amplitudes collected by the dynamic information acquisition system.

3.4 The simulation on the influence of different monitoring positions on the electrical signal

In order to investigate the reasons for the different signal amplitudes collected by the dynamic information acquisition system at different monitoring positions in the experiment of steel plate, this section continues to discuss the impact of PZT actuators and strip sensors at different positions on the received signal amplitudes by establishing a numerical model when the pasting length is fixed.

Using COMSOL software to model the strengthening of steel plates on concrete beams, the three-dimensional elastic wave solid mechanics module was selected for analysis. First, the material properties were set, with concrete, steel plate, and epoxy resin using the materials provided by COMSOL, including Concrete, Structural steel, and Filled epoxy resin (X238). The properties of the materials are shown in Table 5. Then, the pasting length of the steel plate was set to 50%, with the left side being the pasted section and the right side being the debonded section. The constructed three-dimensional model of the steel-reinforced concrete beam is shown in Figure 9. After the model is established, the concrete beam is controlled by the physical field to control the grid, with extremely refined grid divisions. The grid division diagram of the concrete structure is shown in Figure 10.

First, the PZT actuator under the steel-reinforced concrete beam structure is subjected to analysis with a sinusoidal vibration signal source. The amplitude of the sinusoidal signal is 1mm, and the vibration frequency is 500Hz, with specific displacement constraints set. Then, the bottom vibrating block is similarly used as an excitation signal source, utilizing concrete parameters, and the entire structure undergoes transient analysis, with a stop time of 300μs and a step size of 0.1μs. The propagation of stress waves generated by the signal source after its inception is shown in Figure 11.

From Figure 11, it is evident that when the sensor is attached to the left side of the steel plate, i.e., the adhered portion of the steel plate, the stress waves generated by the PZT actuator will rapidly propagate into the concrete due to stress and strain continuity

TABLE 5 Parameters of material performance.

Materials	Density (kg/m3)	Young's modulus (Pa)	Poisson's ratio
Concrete	2,300	2.5×10^{10}	0.2
Steel plate	7,850	2×10^{11}	0.3
Epoxy resin	1730	2.7×10^{5}	0.2

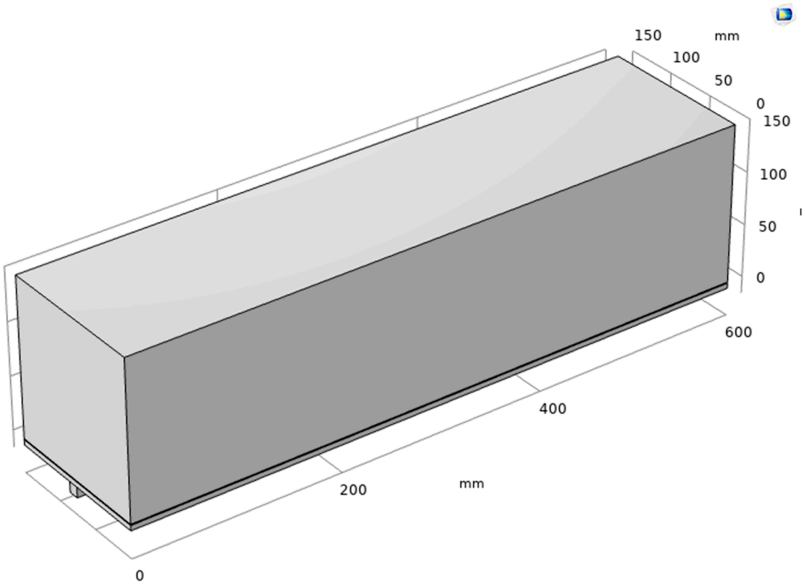

FIGURE 9
Geometric modeling diagram of steel plate reinforced concrete.

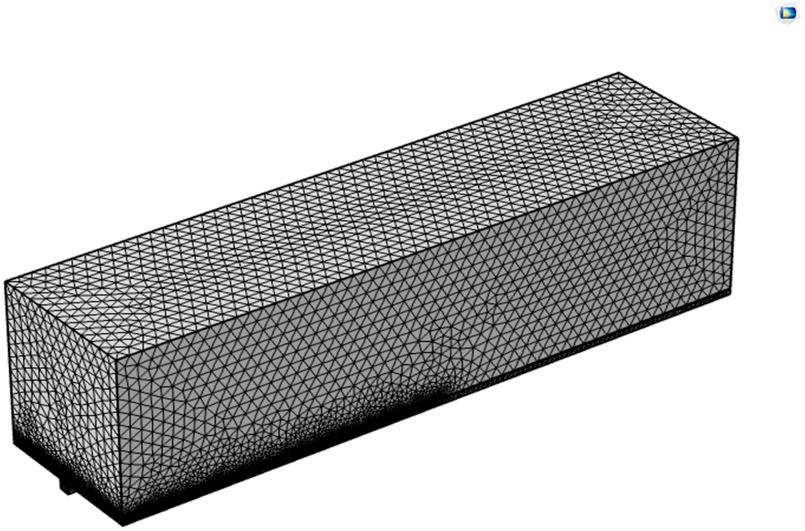

FIGURE 10
Grid division diagram of steel plate reinforced concrete structure.

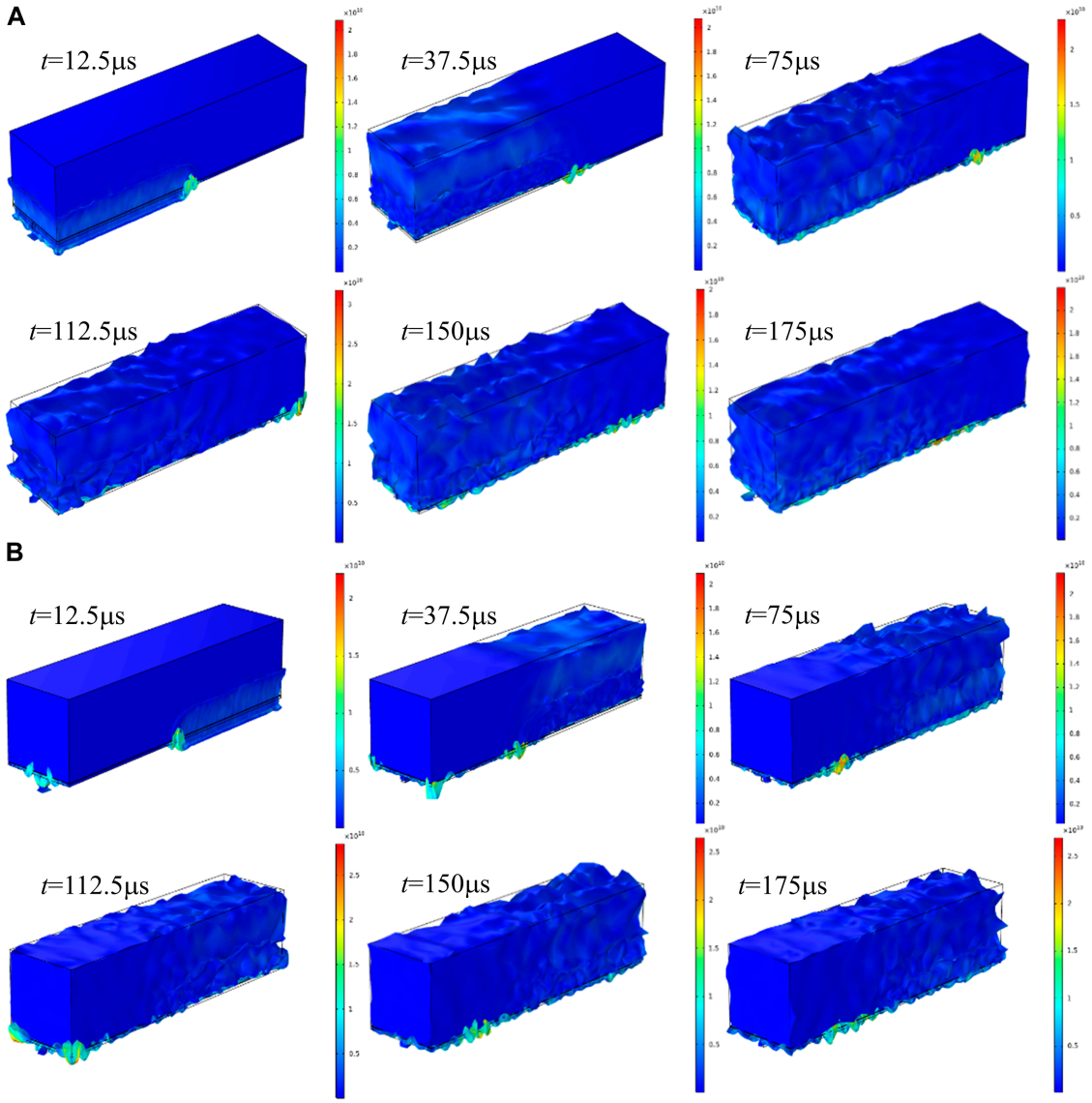

FIGURE 11
The diagram of stress wave propagation. **(A)** Left pasted sensor; **(B)** Right paste sensor.

conditions being met at the adhered region where the steel plate is bonded to the concrete beam with epoxy resin, resulting in stress wave attenuation. When the sensor is attached to the right side of the concrete, i.e., the debonded section of the concrete, the stress waves generated by the PZT actuator first propagate through the steel plate, with a greater range of variation. The majority of the transmitted waves are reflected lback to the strip sensor through the steel plate, and some waves are projected and transmitted into the concrete, causing a rapid reduction in the deformation amplitude of the steel plate. Due to the different forms of energy loss in the adhered and debonded sections of the steel plate, the energy loss in the adhered section is faster, resulting in a smaller signal amplitude in the adhered section. Therefore, the different signal amplitudes captured by the dynamic information acquisition system when the sensor is attached to different positions on the steel plate are due to the different propagation conditions and associated losses during the transmission of stress waves at different positions.

4 Conclusion

In this paper, the active monitoring experiment of steel plate reinforced concrete based on PVDF material is designed. Combined with finite element simulation, the output signal changes of different bond lengths and monitoring positions of steel plates are compared and analyzed, and the debonding law of steel plate-reinforced concrete beams is studied. The main conclusions are as follows:

(1) A piezoelectric theoretical model has been proposed for actively monitoring the degree of concrete debonding of

steel plates. A PZT actuator and a strip sensor using composite materials were prepared to increase the strain range. The voltage signal output by the strip sensor is monitored to evaluate the degree of debonding between the steel plate and the concrete beam by applying an excitation signal to the PZT.

(2) The experiment on active monitoring of bonding between steel plate and reinforced concrete reveals that the signal amplitude received by the strip sensor varies with the degree of debonding of the steel plate when the bonding position of the PZT actuator and strip sensor is fixed. When the length of the paste is 100%, 75%, 50%, and 25%, the output signals of PVDF are 0.017 mV, 0.020 mV, 0.080 mV, and 0.103 mV, respectively. This means that the greater the signal amplitude the strip sensor receives, the greater the degree of debonding between the steel plate and the concrete beam.

(3) Experiments were carried out on concrete beams with different bonding positions of PZT actuators and strip sensors but with the same degree of debonding of steel plates. The results show that under the condition of the same excitation signal, the sensors at different positions have different perceptions of the external signal due to the different external conditions, and the influence of the sensor position change needs to be considered. At this time, the signal received by the sensor installed on the left, middle, and right side, V debonding section > V middle > V pasting section.

(4) The concrete beams with different bonding positions of PZT actuator and strip sensor but the same debonding degree of steel plate were simulated. The simulation results show that the signal amplitude of the strip sensor is different when the sensor is pasted at different positions of the steel plate, which is caused by the different loss of the conduction conditions at different positions in the process of stress wave conduction. The energy loss of the pasting section is fast, so the signal amplitude generated by the pasting section is small.

Data availability statement

The original contributions presented in the study are included in the article/Supplementary Materials, further inquiries can be directed to the corresponding author.

Author contributions

YW: Conceptualization, Methodology, Writing–original draft. HK: Formal Analysis, Software, Writing–original draft. YS: Methodology, Supervision, Writing–original draft. MT: Validation, Writing–original draft. LC: Data curation, Writing–original draft.

Funding

The author(s) declare financial support was received for the research, authorship, and/or publication of this article. This research was funded by the Natural Science Foundation of Chongqing (Grant No. CSTB2022NSCQ-MSX1655) and the State Key Laboratory of Structural Dynamics of Bridge Engineering and Key Laboratory of Bridge Structure Seismic Technology for Transportation Industry Open Fund (Grant No.: 202205).

Conflict of interest

The authors declare that the research was conducted in the absence of any commercial or financial relationships that could be construed as a potential conflict of interest.

Publisher's note

Supplementary material

The Supplementary Material for this article can be found online at: https://www.frontiersin.org/articles/10.3389/fmats.2024.1361159/full#supplementary-material

References

Ali, M. S. M., Oehlers, D. J., and Bradford, M. A. (2005). Debonding of steel plates adhesively bonded to the compression faces of RC beams. *Constr. Build. Mater.* 19 (6), 413–422. doi:10.1016/j.conbuildmat.2004.11.002

Arslan, G., Sevuk, F., and Ekiz, I. (2008). Steel plate contribution to load-carrying capacity of retrofitted RC beams. *Constr. Build. Mater.* 22 (3), 143–153. doi:10.1016/j.conbuildmat.2006.10.009

Aslani, F., and Dehestani, M. (2020). Probabilistic impacts of corrosion on structural failure and performance limits of reinforced concrete beams. *Constr. Build. Mater.* 265, 120316. doi:10.1016/j.conbuildmat.2020.120316

Audrain, P., Masson, P., Berry, A., Pascal, J. C., and Gazengel, B. (2004). The use of PVDF strain sensing in active control of structural intensity in beams. *J. intelligent material Syst. Struct.* 15 (5), 319–327. doi:10.1177/1045389X04039936

Barnes, R. A., and Mays, G. C. (2006). Strengthening of reinforced concrete beams in shear by the use of externally bonded steel plates: Part 2–Design guidelines. *Constr. Build. Mater.* 20 (6), 403–411. doi:10.1016/j.conbuildmat.2005.01.028

Benes, E., Gröschl, M., Burger, W., and Schmid, M. (1995). Sensors based on piezoelectric resonators. *Sensors Actuators A Phys.* 48 (1), 1–21. doi:10.1016/0924-4247(95)00846-2

Bouche, R. R. (1975). "Accelerometers for shock and vibration measurements," in Vibration testing-Instrumentation and data analysis; Proceedings of the Fifth National Vibrations Conference, Washington, D.C. New York, September 17-19 (American Society of Mechanical Engineers), 25–59.

Buda-Ożóg, L., Zięba, J., Sieńkowska, K., Nykiel, D., Zuziak, K., Sieńko, R., et al. (2022). Distributed fibre optic sensing: reinforcement yielding strains and crack

detection in concrete slab during column failure simulation. *Measurement* 195, 111192. doi:10.1016/j.measurement.2022.111192

Dai, J. G., Bai, Y. L., and Teng, J. G. (2011). Behavior and modeling of concrete confined with FRP composites of large deformability. *J. Compos. Constr.* 15 (6), 963–973. doi:10.1061/(ASCE)CC.1943-5614.0000230

Fu, C., and Lao, Y. (2023). Steel–concrete bond deterioration in reinforced concrete tension members due to primary cracks. *Structures* 56, 104895. doi:10.1016/j.istruc.2023.104895

Galkovski, T., Mata-Falcón, J., and Kaufmann, W. (2023). Experimental investigation of bond and crack behaviour of reinforced concrete ties using distributed fibre optical sensing and digital image correlation. *Eng. Struct.* 292, 116467. doi:10.1016/j.engstruct.2023.116467

Hasni, H., Alavi, A. H., Jiao, P., Lajnef, N., Chatti, K., Aono, K., et al. (2017). A new approach for damage detection in asphalt concrete pavements using battery-free wireless sensors with non-constant injection rates. *Measurement* 110, 217–229. doi:10.1016/j.measurement.2017.06.035

Hawileh, R. A., Nawaz, W., and Abdalla, J. A. (2018). Flexural behavior of reinforced concrete beams externally strengthened with Hardwire Steel-Fiber sheets. *Constr. Build. Mater.* 172, 562–573. doi:10.1016/j.conbuildmat.2018.03.225

Howser, R., Moslehy, Y., Gu, H., Dhonde, H., Mo, Y. L., Ayoub, A., et al. (2011). Smart-aggregate-based damage detection of fiber-reinforced-polymer-strengthened columns under reversed cyclic loading. *Smart Mater. Struct.* 20 (7), 075014. doi:10.1088/0964-1726/20/7/075014

Huo, L., Li, C., Jiang, T., and Li, H. N. (2018). Feasibility study of steel bar corrosion monitoring using a piezoceramic transducer enabled time reversal method. *Appl. Sci.* 8 (11), 2304. doi:10.3390/app8112304

Jones, R., Swamy, R. N., and Charif, A. (1988). Plate separation and anchorage of reinforced concrete beams strengthened by epoxy-bonded steel plates. *Struct. Eng.* 66 (5). Available at: http://worldcat.org/issn/14665123.

Kaklauskas, G. (2017). Crack model for RC members based on compatibility of stress-transfer and mean-strain approaches. *J. Struct. Eng.* 143 (9), 04017105. doi:10.1061/(ASCE)ST.1943-541X.0001842

Kumar, A., Varghese, A., Sharma, A., Prasad, M., Janyani, V., Yadav, R., et al. (2022). Recent development and futuristic applications of MEMS based piezoelectric microphones. *Sensors Actuators A Phys.* 2022, 113887. doi:10.1016/j.sna.2022.113887

Li, Y. Y., Guo, B., and Liu, J. (2014). Research on reinforced concrete beam enlarged cross section method experiment and finite element simulation. *Appl. Mech. Mater.* 638, 208–213. doi:10.4028/www.scientific.net/AMM.638-640.208

Liao, W. I., Gu, H., Olmi, C., Song, G., Mo, Y. L., and Loh, C. H. (2008). Structural health monitoring of a concrete column subjected to shake table excitations using smart aggregates. *Earth Space* 2008, 1–8. doi:10.1061/40988(323)169

Ma, X., and Liu, L. (2023). Fatigue properties of RC beams reinforced with ECC layer and steel plate. *Constr. Build. Mater.* 372, 130799. doi:10.1016/j.conbuildmat.2023.130799

Naser, M. Z., Hawileh, R. A., and Abdalla, J. A. (2019). Fiber-reinforced polymer composites in strengthening reinforced concrete structures: a critical review. *Eng. Struct.* 198, 109542. doi:10.1016/j.engstruct.2019.109542

Oehlers, D. J., and Ali, M. S. M. (1998). Debonding of steel plates glued to RC flexural members. *Prog. Struct. Eng. Mater.* 1 (2), 185–192. doi:10.1002/pse.2260010211

Othmani, C., Zhang, H., and Lü, C. (2020). Effects of initial stresses on guided wave propagation in multilayered PZT-4/PZT-5A composites: a polynomial expansion approach. *Appl. Math. Model.* 78, 148–168. doi:10.1016/j.apm.2019.10.017

Prabakar, K. (2007). Acoustic emission from PZT-5A and PZT-8 ceramics during the application of AC field at different frequencies. *Int. J. Mod. Phys. B* 21 (27), 4707–4714. doi:10.1142/S0217979207038095

Qin, F., Kong, Q., Li, M., Mo, Y. L., Song, G., and Fan, F. (2015). Bond slip detection of steel plate and concrete beams using smart aggregates. *Smart Mater. Struct.* 24 (11), 115039. doi:10.1088/0964-1726/24/11/115039

Qu, Y., Liu, W., Gwarzo, M., Zhang, W., Zhai, C., and Kong, X. (2017). Parametric study of anti-explosion performance of reinforced concrete T-shaped beam strengthened with steel plates. *Constr. Build. Mater.* 156, 692–707. doi:10.1016/j.conbuildmat.2017.08.150

Shah, A. A., and Ribakov, Y. (2009). Non-linear ultrasonic evaluation of damaged concrete based on higher order harmonic generation. *Mater. Des.* 30 (10), 4095–4102. doi:10.1016/j.matdes.2009.05.009

Shah, A. A., Ribakov, Y., and Hirose, S. (2009). Nondestructive evaluation of damaged concrete using nonlinear ultrasonics. *Mater. Des.* 30 (3), 775–782. doi:10.1016/j.matdes.2008.05.069

Song, G., Qiao, P. Z., Binienda, W. K., and Zou, G. P. (2002). Active vibration damping of composite beam using smart sensors and actuators. *J. Aerosp. Eng.* 15 (3), 97–103. doi:10.1061/(ASCE)0893-1321(2002)15:3(97)

Wu, A., He, S., Ren, Y., Wang, N., Ho, S., and Song, G. (2019). Design of a new stress wave-based pulse position modulation (PPM) communication system with piezoceramic transducers. *Sensors* 19 (3), 558. doi:10.3390/s19030558

Xu, K., Ren, C., Deng, Q., Jin, Q., and Chen, X. (2018). Real-time monitoring of bond slip between GFRP bar and concrete structure using piezoceramic transducer-enabled active sensing. *Sensors* 18 (8), 2653. doi:10.3390/s18082653

Yang, J., Chen, R., Zhang, Z., Zou, Y., Zhou, J., and Xia, J. (2023). Experimental study on the ultimate bearing capacity of damaged RC arches strengthened with ultra-high performance concrete. *Eng. Struct.* 279, 115611. doi:10.1016/j.engstruct.2023.115611

Ye, Y., Laishun, Z., and Man, Z. (2010). Experimental investigation of axial compression column be strengthened with the method of enlarging sectional areas. *Build. Struct.* 40 (6), 412–414. doi:10.19701/j.jzjg.2010.s2.122

Yu, Y., Zhao, X., Wang, Y., and Ou, J. (2013). A study on PVDF sensor using wireless experimental system for bridge structural local monitoring. *Telecommun. Syst.* 52, 2357–2366. doi:10.1007/s11235-011-9558-5

Zaki, Y. A., Abouhussien, A. A., Hassan, A. A. A., et al. (2023). Crack detection and classification of repaired concrete beams by acoustic emission monitoring. *Ultrasonics* 2023, 107068. doi:10.1016/j.ultras.2023.107068

Zanuy, C., de la Fuente, P., and Albajar, L. (2007). Effect of fatigue degradation of the compression zone of concrete in reinforced concrete sections. *Eng. Struct.* 29 (11), 2908–2920. doi:10.1016/j.engstruct.2007.01.030

Zeng, L., Parvasi, S. M., Kong, Q., Huo, L., Lim, I., Li, M., et al. (2015). Bond slip detection of concrete-encased composite structure using shear wave based active sensing approach. *Smart Mater. Struct.* 24 (12), 125026. doi:10.1088/0964-1726/24/12/125026

Zhan, T., Wang, Z., and Ning, J. (2015). Failure behaviors of reinforced concrete beams subjected to high impact loading. *Eng. Fail. Anal.* 56, 233–243. doi:10.1016/j.engfailanal.2015.02.006

Zhang, Y., Tang, L., Tian, H., Wang, J., Cao, W., and Zhang, Z. (2017). Determination of temperature dependence of full matrix material constants of PZT-8 piezoceramics using only one sample. *J. alloys Compd.* 714, 20–25. doi:10.1016/j.jallcom.2017.04.124

Zhang, Z., Pang, K., Xu, L., Zou, Y., Yang, J., and Wang, C. (2023). The bond properties between UHPC and stone under different interface treatment methods. *Constr. Build. Mater.* 365, 130092. doi:10.1016/j.conbuildmat.2022.130092

Zhao, X., and Li, H. (2006). Health monitoring of reinforced concrete frame-shear wall using piezoceramic transducer. *J. Vib. Shock* 25 (4), 82–84. doi:10.13465/j.cnki.jvs.2006.04.022

Zou, Y., Jiang, J., Yang, J., Zhang, Z., and Guo, J. (2023). Enhancing the toughness of bonding interface in steel-UHPC composite structure through fiber bridging. *Cem. Concr. Compos.* 137, 104947. doi:10.1016/j.cemconcomp.2023.104947